Quantum Fluctuations, Temperature, and Detuning Effects in Solid-Light Systems

Markus Aichhorn,[1] Martin Hohenadler,[2] Charles Tahan,[2,3] and Peter B. Littlewood[2]

[1]*Institute for Theoretical Physics and Astrophysics, University of Würzburg, Germany*

[2]*Theory of Condensed Matter, Cavendish Laboratory, University of Cambridge, Cambridge CB3 0HE, United Kingdom*

[3]*Booz Allen Hamilton Inc., 3811 N. Fairfax Dr., Arlington, Virginia 22203, USA*

(Received 14 February 2008; revised manuscript received 27 March 2008; published 29 May 2008)

The superfluid to Mott insulator transition in cavity polariton arrays is analyzed using the variational cluster approach, taking into account quantum fluctuations exactly on finite length scales. Phase diagrams in one and two dimensions exhibit important non-mean-field features. Single-particle excitation spectra in the Mott phase are dominated by particle and hole bands separated by a Mott gap. In contrast to Bose-Hubbard models, detuning allows for changing the nature of the bosonic particles from quasilocalized excitons to polaritons to weakly interacting photons. The Mott state with density one exists up to temperatures $T/g \gtrsim 0.03$, implying experimentally accessible temperatures for realistic cavity couplings g.

DOI: 10.1103/PhysRevLett.100.216401 PACS numbers: 71.36.+c, 42.50.Ct, 73.43.Nq, 78.20.Bh

The prospect of realizing a tunable, strongly correlated system of photons is exciting, both as a testbed for quantum many-body dynamics and for the potential of quantum simulators and other advanced quantum devices. Three proposals based on cavity-QED arrays have recently shown how this might be accomplished [1–3], followed by further work [4–8]. Engineered strong photon-photon interactions and hopping between cavities allow photons (as a component of cavity polaritons) to behave much like electrons or atoms in a many-body context. It is clear that a particular signature of quantum many-body physics, the superfluid (SF) to Mott insulator (MI) transition, should be reproducible in such systems and be similar to the widely studied Bose-Hubbard model (BHM). Yet, the BH analogy is not complete. The mixed matter-light nature of the system brings new physics yet to be fully explored.

"Solid-light" systems—so-named for the intriguing MI state of photons they exhibit—are reminiscent of cold atom optical lattices (CAOL) [9], but have some advantages concerning direct addressing of individual sites and device integration, and the potential for asymmetry construction by individual tuning, local variation, and far from equilibrium devices [4]. Photons as part of the system serve as excellent experimental probes, and have excellent "flying" potential so that they can be transported over long distances. Temporal and spatial correlation functions are accessible, and nonequilibrium quantum dynamics may be studied using coherent laser pumping to create initial states. The possible implementations are many [1]. In particular, microcavities linked by optical fibers [2,10], small arrays of stripline superconducting Cooper-pair boxes or "transmon" cavities [1,11], condensate arrays [12] and color center or quantum dot periodic band-gap (PBG) materials [1,5] seem most promising.

Here we focus on the simplest solid-light model [1], describing L optical microcavities each containing a single two-level atom with states $|\downarrow\rangle$, $|\uparrow\rangle$ separated by energy ϵ. The Hamiltonian reads ($\hbar = 1$)

$$\hat{H} = -t\sum_{\langle i,j\rangle} a_i^\dagger a_j + \sum_i \hat{H}_i^{\mathrm{JC}} - \mu\hat{N}_p,$$
$$\hat{H}_i^{\mathrm{JC}} = \epsilon|\uparrow_i\rangle\langle\uparrow_i| + \omega_0 a_i^\dagger a_i + g(|\uparrow_i\rangle\langle\downarrow_i|a_i + |\downarrow_i\rangle\langle\uparrow_i|a_i^\dagger). \quad (1)$$

Here ω_0 is the cavity photon energy, and $\Delta = \omega_0 - \epsilon$ defines the detuning. Each cavity is described by the well-known Jaynes-Cummings (JC) Hamiltonian $\hat{H}^{\mathrm{JC}}$. The atom-photon coupling g ($a_i^\dagger$, a_i are photon creation and annihilation operators) gives rise to formation of polaritons (combined atom-photon excitations) whose number $\hat{N}_p = \sum_i (a_i^\dagger a_i + |\uparrow_i\rangle\langle\uparrow_i|)$ is conserved and couples to the chemical potential μ [7]. We consider nearest-neighbor photon hopping with amplitude t, define the polariton density $n = \langle N_p\rangle/L$, use g as the unit of energy and set ω_0/g [13], k_B and the lattice constant to one.

Hamiltonian (1) represents a generic model of strongly correlated photons amenable to numerical methods. Existing theoretical work has focused on mean-field calculations [1], exact diagonalization of few-cavity systems [2,3,7], and the 1D case [8]. Here we employ a quantum many-body method for the thermodynamic limit to explore the physics of the model. In particular, quantum fluctuations on a finite length scale are included. We discuss Mott lobes (also at experimentally relevant finite temperatures), the effect of detuning and for the first time in such systems calculate single-particle spectra, a necessary connection to experiment and also a key metric in early proof of concept calculations of CAOL systems.

The variational cluster approach (VCA)—introduced first for strongly correlated electrons [14]—has previously been applied to the BHM [15]. The main idea is to approximate the self-energy $\mathbf{\Sigma}$ of the infinite system by that of a finite reference system. The matrix notation includes orbitals and bosonic Matsubara frequencies, $\mathbf{\Sigma} = \Sigma_{\alpha\beta}(i\omega_n)$. The optimal choice for $\mathbf{\Sigma}$ follows from a general variational principle $\delta\Omega[\mathbf{\Sigma}] = 0$, Ω being the grand potential. Trial self-energies from isolated clusters (with

L_c sites) are parametrized by the one-particle parameters $\boldsymbol{\xi}^c = \{t^c, \epsilon^c, \omega_0^c, \mu^c\}$ of the reference-system Hamiltonian, i.e., $\boldsymbol{\Sigma} = \boldsymbol{\Sigma}(\boldsymbol{\xi}^c)$. For bosons [15],

$$\Omega = \Omega^c + \mathrm{Tr}\ln(\boldsymbol{G}_0^{-1} - \boldsymbol{\Sigma})^{-1} - \mathrm{Tr}\ln(\boldsymbol{G}^c). \qquad (2)$$

Here, Ω^c, $\boldsymbol{G}^c$, and $\boldsymbol{\Sigma}$ are the grand potential, Green's function, and self-energy of an isolated cluster, and $\boldsymbol{G}_0$ is the noninteracting ($g = 0$) Green's function. $\boldsymbol{G}_0$, $\boldsymbol{G}^c$, and $\boldsymbol{\Sigma}$ are evaluated at bosonic Matsubara frequencies $i\omega_n$, and traces include frequency summation. The stationary solution is given by $\partial\Omega/\partial\boldsymbol{\xi}^c = 0$. Traces can be evaluated exactly using only the poles of the Green's function but not their weights [14,15]. The poles ω_m of $\boldsymbol{G}_0^{-1} - \boldsymbol{\Sigma}$ are obtained from a bosonic formulation of the Q-matrix method [16]. At temperature $T > 0$, the required matrix diagonalization restricts L_c and $T_{\max}$. For simplicity, we restrict ourselves to a single variational parameter $\xi^c = \omega_0^c$.

The full quantum dynamics are taken into account exactly on the length scale of the cluster L_c, and even for $L_c = 1$ VCA results are beyond the mean-field solution [1,15]. The present formulation cannot describe the properties of the SF phase, as the required symmetry-breaking term $\hat{H}_\psi = \psi\sum_i(a_i^\dagger + a_i)$ cannot be cast into a single-particle operator. However, this does not affect the accuracy of the phase boundary of the MI. The numerical effort is very moderate as compared to, e.g., the density matrix renormalization group [8], and the VCA provides $T = 0$ and $T > 0$ static and dynamic properties in one and two dimensions.

The $T = 0$ phase diagram in one (chain) and two dimensions (square lattice) is shown in Fig. 1. There exists a series of Mott lobes with integer polariton density $n_{\mathrm{int}} = 0, 1, \ldots$ and compressibility $\kappa \equiv \partial n/\partial\mu = 0$ [1]. In contrast to recently proposed photonic MI phases [4], $\langle a^\dagger a\rangle$ fluctuates even for constant, integer n. Inside the lobes, where the VCA yields a solution, the system has an energy gap $\tilde{E}_{g,p}$ ($\tilde{E}_{g,h}$) for adding a particle (hole) equal to the vertical distance of μ from the upper (lower) phase boundary [17]. The spacing of the points $\mu_n = \omega_0 + g(\sqrt{n} - \sqrt{n+1})$ where adjacent lobes touch at $t/g = 0$ decreases quickly with increasing n, in contrast to the BHM where $\mu_n = Un$. Convergence with cluster size L_c is surprisingly fast. The 1D data agree well with exact results, although the VCA slightly underestimates t^* (the value of t at the lobe tip, $t^*/g = 0.2$ in [8]). Figure 1(b) represents the first accurate (non-mean-field) phase diagram in two dimensions, arguably the most important case for experimental realizations.

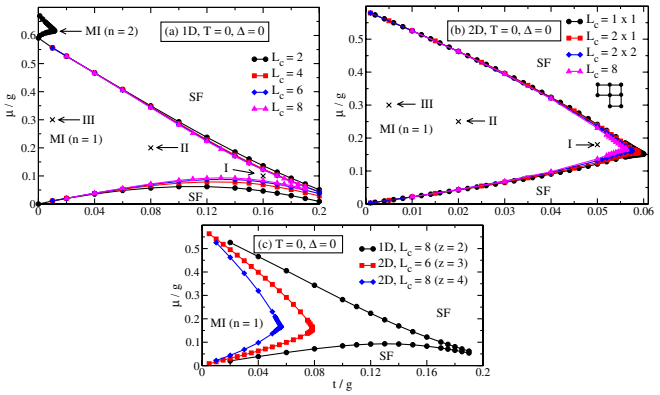

FIG. 1 (color online). Ground-state phase diagram: (a) 1D, (b) 2D, and (c) different coordination numbers z. Lines are guides to the eye.

For $t/g = 0$, the MI states are $\prod_i|\psi_n\rangle_i$, where the n-polariton eigenstate of $\hat{H}^{\mathrm{JC}}$ (the $|-, n\rangle$ branch in [1]) is a superposition of photonic ($|\downarrow, n\rangle$, with n photons) and excitonic states ($|\uparrow, n-1\rangle$),

$$|\psi_n\rangle = \eta(\Delta, n)|\downarrow, n\rangle + \phi(\Delta, n)|\uparrow, n-1\rangle. \qquad (3)$$

Lobes with $n > 1$ are much smaller due to the effective polariton repulsion decreasing with n, and we focus on the $n = 1$ case for which quantum effects are strongest, and which can be easily initialized experimentally.

Figures 1(a) and 1(b) show significant deviations from the parabolic lobes predicted by mean-field theory in both one and two dimensions. However, quantum fluctuation effects diminish quickly with increasing coordination number z [Fig. 1(c)]. In particular, the reentrant behavior with increasing t/g [18] and the cusplike tip indicative of the Berezinskii-Kosterlitz-Thouless transition [19] exist only for $z = 2$.

Spectral properties play a key role in understanding condensed matter systems, but are notoriously difficult to calculate accurately. In cavities, the occupation and spectra can be directly monitored through luminescence spectra, with angular emission translating into momentum $\boldsymbol{k}$, much more straightforward than in CAOL.

The VCA yields the single-particle spectral function $A(k, \omega) = -\pi^{-1}\mathrm{Im}G(k, \omega)$, shown in Fig. 2 for the pa-

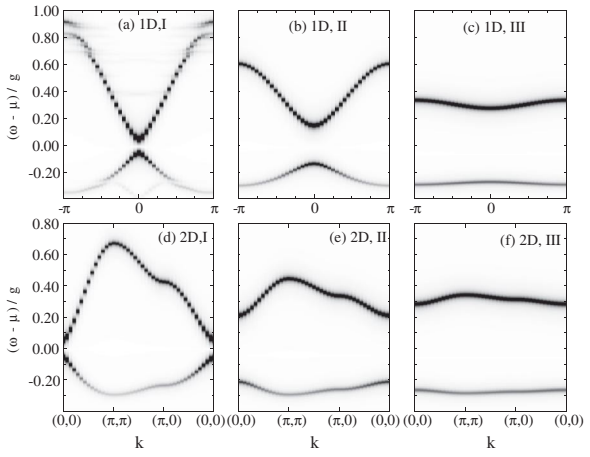

FIG. 2. Single-particle spectra at $T = 0$ in one dimension [(a)–(c), $L_c = 6$] and 2D [(d)–(f), $L_c = 2 \times 2$]. I–III refer to the marks in Fig. 1, i.e., (a) $t/g = 0.16$, (b) 0.08, (c) 0.01, (d) 0.05, (e) 0.02, (f) 0.005.

rameters marked in Fig. 1. Important for detection in experiment, the MI state is characterized by cosinelike particle and hole bands, separated by the Mott gap E_g, minimal at $\boldsymbol{k} = 0$, which decreases with increasing t/g, and eventually closes in the SF phase. The phase boundaries $\mu_\pm$ are related to the particle or hole dispersions $\varepsilon_{p/h}(\boldsymbol{k} = 0, t)$ via $\mu_+(t) = \varepsilon_p(0, t)$ and $\mu_-(t) = \varepsilon_h(0, t)$, and the Mott gap is given by $E_g(t) = \varepsilon_p(0, t) - \varepsilon_h(0, t)$ [20].

For $t \ll t^*$, particles are much lighter than holes (e.g., $tm_p \approx 0.33$, $tm_h \approx 0.81$ in Fig. 2(c); obtained from parabolic fits). The particle or hole bandwidth scales almost linearly with t, confirming the weakly interacting Bose gas picture for the superfluid fraction of particles/holes doped into the MI [19]. The hole bandwidth in both one and two dimensions is about zt. For the BHM model, the ratio of the bandwidths is $W_p/W_h = 2$ for the MI with $n = 1$ due to the effective particle (hole) hopping $t_p = (n + 1)t$ ($t_h = nt$) [15,21]. For the JCM, the matrix elements for hopping of one particle or hole in the MI have to be evaluated using the dressed states $|\psi_n\rangle$, and we find $W_p/W_h = 3/2 + \sqrt{2} \approx 2.91$ in one dimension, in good agreement with Figs. 2(a)–2(c). The bandwidth ratio is fairly independent of t/U, respectively, t/g because the interaction energy of a single particle or hole is the same at every site. In the BHM, emergent particle-hole symmetry leads to $m_p \approx m_h \to 0$ for $t \to t^*$ [22]. This behavior is also seen in the JCM ($m_p/m_h \approx 1.3$ for $t = 0.16$ in 1D), but the VCA does not permit a detailed analysis near t^*.

In contrast to CAOL, the parameters ϵ and ω_0 and hence the detuning $\Delta = \epsilon - \omega_0$ can easily be changed experimentally. This permits to tune the character of the bosonic particles. The states $|\psi_n\rangle$ are excitonlike for $\omega_0 \gg \epsilon$, photonlike for $\omega_0 \ll \epsilon$, and polaritonlike for $\omega_0 \approx \epsilon$. The 1D phase diagrams for $\Delta/g = \pm 2$ are shown in Figs. 3(a) and 3(b). The excitonic system ($\Delta/g = 2$) with small photon-mediated hopping exhibits a large $n = 1$ Mott lobe, whereas the latter is very small in the photonic system with small exciton-mediated interaction. Reentrant behavior due to quantum fluctuations is seen for the excitonic case, but is absent in the photonic case for large enough L_c.

Single-particle spectra in one dimension near the lobe tips are shown in Fig. 3(c) and 3(d). The excitonic system shows a very large ratio of particle and hole bandwidths ($W_p/W_h \approx 7$), whereas $W_p/W_h \approx 2.1$ (very close to the BHM, since $|\psi_1\rangle \approx |\downarrow, 1\rangle$) for the photonic case. These values result from the different admixture of the states $|\uparrow, 0\rangle$ and $|\downarrow, 1\rangle$ to $|\psi_1\rangle$ depending on Δ. In particular, the approximate relation $W_h \approx zt$ found for $\Delta = 0$ does not hold. The excitonic MI with $n = 1$ is approximately given by $\prod_i |\uparrow, 0\rangle_i$, whereas we have $\prod_i |\downarrow, 1\rangle_i$ for the photonic case. Finally, the incoherent features in Fig. 3(c) may originate from the finite cluster size L_c, and should be addressed using other exact methods.

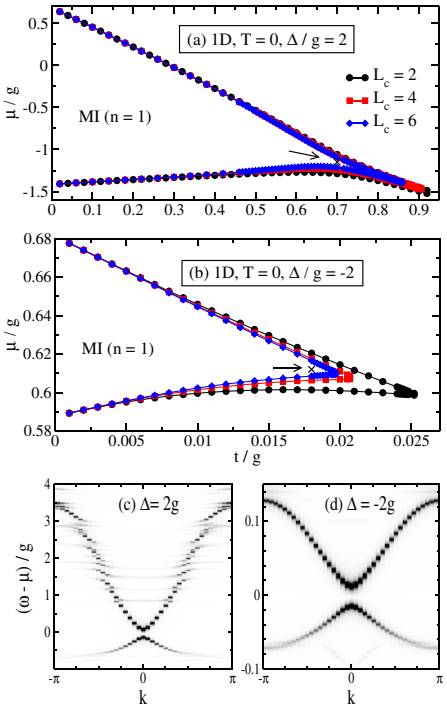

FIG. 3 (color online). Phase diagram for detuning (a) $\Delta/g = -2$, (b) $\Delta/g = 2$, and spectra for (c) $\Delta/g = 2$, $t/g = 0.7$, and (d) $\Delta/g = -2$, $t/g = 0.0.018$ in one dimension at $T = 0$.

Solid state quantum devices will operate at finite temperature, much higher than in CAOL (estimated at nK). This leads to the important question of the stability of the MI state at $T > 0$, which will ultimately determine their technological usefulness. Strictly speaking, there is no true MI at $T > 0$ due to thermal fluctuations. However, there exist regions where fluctuations are small enough for the system to behave like a MI for experimental purposes [23]. We determine the region of existence of the MI using the stringent criterion $\Delta n = |n - n_{\text{int}}| \leq 10^{-4}$, corresponding to a ''worst case scenario'', since experimentally the MI will survive as long as the Mott gap $\sim g$ is large compared to thermal fluctuations.

Results for $\Delta = 0$ are shown for one and two dimensions in Fig. 4. Finite-size effects diminish quickly with increasing temperature [see Fig. 4(a)]. The size of the $n = 1$ Mott lobe is significantly reduced with increasing temperature, and Δn exceeds 10^{-4} at $T^*/g \approx 0.03$ in both one and two dimensions. This value is consistent with the onset of deviations of n from 1 in the exact atomic-limit results, and agrees with the few-cavity results of [7]. Lobes with $n > 1$ disappear at much lower temperatures (not shown). In contrast to $T = 0$, Mott lobes with n and $n \pm 1$ do not touch at $t/g = 0$, but are surrounded by the normal fluid (NF) phase for sufficiently small t/g, and a transition NF-SF occurs at larger t/g. However, while the VCA can distinguish between the MI and the NF, the phase boundary to the SF at $T > 0$ cannot be determined accurately. The gap in $A(\boldsymbol{k}, \omega)$ increases with T [23]. Particle or hole bands

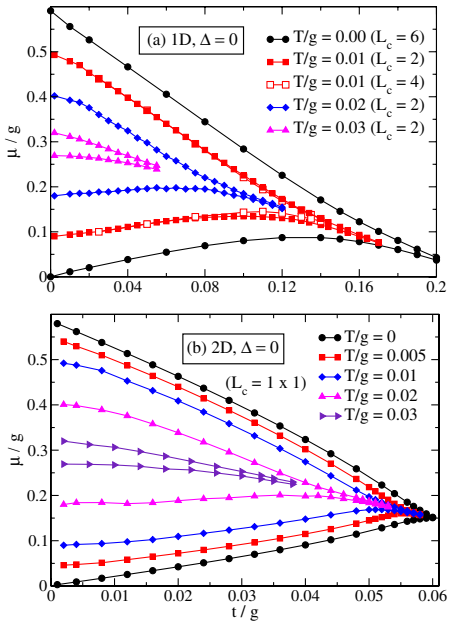

FIG. 4 (color online). Mott-like regions for different T.

are still well defined at $T > 0$, and spectra (not shown) look very similar to $T = 0$. Excitation spectra of the NF and SF deserve detailed future studies.

The quasi-MI lobes in Fig. 4 are dominated by the point ($t = 0$, $\mu \approx 0.3$) where $\tilde{E}_g$ is maximal and by the $T = 0$ lobe tip (μ^*, t^*). The MI is destroyed by thermal excitation of particles or holes, and therefore survives longest near $\mu = 0.3$ where the energy cost is largest. Besides, T^* is determined by the size of the lobe at $T = 0$, $t = 0$. Hence, the system at $T > 0$ is dominated by atomic-limit physics (yielding the same T^* in 1D and 2D) and the $T = 0$ fixed point (quantum critical point) of the MI-SF transition [19]. For the 1D BHM [19], the VCA yields $T^*/U \approx 0.059$, lower than $T^*/U = 0.2$ found in [24] using a different criterion [25]. The ratio of the critical temperatures for the 1D JCM and 1D BHM is 0.56, close to the ratio of the $t = 0$, $T = 0$ Mott gaps (0.59).

Solid state cavity-QED systems offer the possibility of large g. Taking a conservative estimate $g = 10^{10}$ Hz [1] gives for the effective temperature of the quantum system $T^* \gtrsim 14$ mK. Even taken as the actual temperature, this is well accessible experimentally. The hopping rate $1/t$ has to be fast enough to permit equilibration before photon loss and dephasing set in. Indeed, taking $t/g = 0.01$ (inside the Mott lobe in Fig. 4(b)], we obtain a realistic $t^{-1} \gtrsim 0.14$ ps. Finally, T^* for the $n = 1$ MI is enhanced by detuning $\Delta > 0$ [Fig. 3(a)], which additionally increases t^* and $|\mu^*|$, estimated as $(\mu^*, t^*) \approx (0.08, 0.02)$ meV in two dimensions for $T = \Delta = 0$.

In summary, motivated by theoretical predictions and ongoing experimental advances, we have studied polariton Mott phases by means of a versatile quantum many-body approach. Phase diagrams, single-particle spectra and finite temperature effects have been related to the known features of Bose-Hubbard models and possible experiments, and the novel physics emerging from detuning has been explored.

This work was supported by the FWF Schrödinger Grant No. J2583, the DFG research unit FOR538, and by NSF Grant No. DMR-0502047. C. T. would like to acknowledge useful conversations with A. Greentree *et al*.

[1] A. D. Greentree, C. Tahan, J. H. Cole, and L. C. L. Hollenberg, Nature Phys. **2**, 856 (2006).
[2] M. J. Hartmann, F. G. S. L. Brandão, and M. B. Plenio, Nature Phys. **2**, 849 (2006).
[3] D. G. Angelakis, M. F. Santos, and S. Bose, Phys. Rev. A **76**, 031805(R) (2007).
[4] M. J. Hartmann and M. B. Plenio, Phys. Rev. Lett. **99**, 103601 (2007); Phys. Rev. Lett. **100**, 070602 (2008).
[5] N. Na, S. Utsunomiya, L. Tian, and Y. Yamamoto, Phys. Rev. A **77**, 031803(R) (2008).
[6] S.-C. Lei and R.-K. Lee, Phys. Rev. A **77**, 033827 (2008).
[7] M. I. Makin, J. H. Cole, C. Tahan, L. C. L. Hollenberg, and A. D. Greentree, arXiv:0710.5748 [Phys. Rev. A (to be published)].
[8] D. Rossini and R. Fazio, Phys. Rev. Lett. **99**, 186401 (2007).
[9] M. Lewenstein, A. Sanpera, V. Ahufinger, B. Damski, A. Sen, and U. Sen, Adv. Phys. **56**, 243 (2007).
[10] D. E. Chang, V. Gritsev, G. Morigi, V. Vuletic, M. D. Lukin, and E. A. Demler, arXiv:0712.1817 (unpublished).
[11] J. Koch, T. M. Yu, J. Gambetta, A. A. Houck, D. I. Schuster, J. Majer, A. Blais, M. H. Devoret, S. M. Girvin, and R. J. Schoelkopf, Phys. Rev. A **76**, 042319 (2007).
[12] C. W. Lai, N. Y. Kim, S. Utsunomiya, G. Roumpos, H. Deng, M. D. Fraser, T. Byrnes, P. Recher, N. Kumada, T. Fujisawa, and Y. Yamamoto, Nature (London) **450**, 529 (2007).
[13] As in [1]; ω_0 is not an absolute frequency, so that this choice does not affect results.
[14] M. Potthoff, M. Aichhorn, and C. Dahnken, Phys. Rev. Lett. **91**, 206402 (2003); M. Potthoff, Eur. Phys. J. B **36**, 335 (2003).
[15] W. Koller and N. Dupuis, J. Phys. Condens. Matter **18**, 9525 (2006).
[16] M. Aichhorn, E. Arrigoni, M. Potthoff, and W. Hanke, Phys. Rev. B **74**, 235117 (2006).
[17] For $t/g = 0$ and density n, a particle or hole corresponds to one site having occupation $n + 1$ ($n - 1$).
[18] T. D. Kühner and H. Monien, Phys. Rev. B **58**, R14741 (1998).
[19] M. P. A. Fisher, P. B. Weichman, G. Grinstein, and D. S. Fisher, Phys. Rev. B **40**, 546 (1989).
[20] N. Elstner and H. Monien, Phys. Rev. B **59**, 12 184 (1999).
[21] D. van Oosten, P. van der Straten, and H. T. C. Stoof, Phys. Rev. A **63**, 053601 (2001).
[22] B. Capogrosso-Sansone, N. V. Prokof'ev, and B. V. Svistunov, Phys. Rev. B **75**, 134302 (2007).
[23] D. van Oosten, P. van der Straten, and H. T. C. Stoof, Phys. Rev. A **67**, 033606 (2003).
[24] F. Gerbier, Phys. Rev. Lett. **99**, 120405 (2007).
[25] There are no well-defined plateaus in the density even below $T^*/U = 0.2$ in [24].